ELSEVIER

International Journal of Heat and Fluid Flow 20 (1999) 605–613

International Journal of HEAT AND FLUID FLOW

www.elsevier.com/locate/ijhff

Transient removal of a contaminated fluid from a cavity

L.C. Fang [a,*], D. Nicolaou [b], J.W. Cleaver [b]

[a] *Chinese Military Academy, PO Box 90602-6, Fengshan, Kaohsiung 830, Taiwan, ROC*

[b] *Department of Engineering, University of Liverpool, Mechanical Engineering Building, Brownlow Street, Liverpool L69 3GH, UK*

Received 24 March 1998; accepted 2 May 1999

Abstract

A numerical and experimental study of the time-dependent hydrodynamic removal of a contaminated fluid from a cavity on the floor of a duct is presented. The duct flow has a parabolic inlet velocity profile and laminar flows are considered in a Reynolds number range between 50 and 1600 based on the duct height. The properties of the contaminated cavity fluid are assumed to be the same as for the fluid flowing in the duct. Attention is focussed on the convective transport of contaminated fluid out from the cavity and the effect of duct flow acceleration on the cleaning process. Passive markers which are convected with the flow are used in the numerical simulation for the purpose of identifying the contaminated cavity fluid. It is shown that the cleansing of the cavity is more pronounced during the unsteady start-up of the duct flow and the rate of cleaning decreases as the flow reaches a steady state. The cleaning process is enhanced as the cavity aspect ratio is increased and as the duct Reynolds number increases. A 'volumetric' approach based on the spread of markers is shown to be useful in determining the fraction of the cavity that remains contaminated after steady conditions have been reached. The distribution of the contaminant in a cavity during the unsteady stage and after steady conditions are reached are identified using passive markers.

Keywords: Cavity; Duct; Numerical; Laminar; Cleaning; Navier–Stokes; Transient; Unsteady

1. Introduction

The hydrodynamic or aerodynamic removal of a fluid foulant from the internal surfaces of process equipment is very dependent on the roughness of the surface finish and any large scale cavities which may arise through poorly fitted components and junctions in the pipework. This was highlighted by the work of Mickaily and Middleman (1993) who measured the efficiency of aerodynamic cleaning of oil from the inside of pipelines. Using a simple model based on the removal of a deformable fluid foulant from a smooth surface by a steady shear flow they showed good agreement with experiments for most of the cleaning period but failed to predict the long term behaviour of the foulant. This was attributed to foulant being trapped within small cavities embedded in the surface. By modelling a flow over a rough surface, using the analogy of a Couette flow over a fluid contained in a cavity, they were able to improve the prediction of the maximum amount of foulant which can be removed.

In earlier work Chilukuri and Middleman (1983) addressed the problem of mass diffusion from a cavity which is initially full of the same fluid as the flushing fluid but which contains a specified concentration of a contaminant. Assuming that the fluid in the cavity does not interact with the cleaning fluid and that the interface is straight they assess the influence of the recirculating flow in the cavity on the removal of the contaminant by molecular diffusion. This is achieved by assuming that the Navier–Stokes equations are decoupled from the mass transfer equations and that the velocity components in the cavity are those which exist in steady state conditions. The analysis clearly shows that the secondary flow in the cavity enhances mass transfer by molecular diffusion from the cavity by an order of magnitude or more and that it is a maximum when the cavity aspect ratio (width/depth) is about 1.5.

Table 1, although not extensive, shows the breadth of parameters which have been considered by previous studies on steady flows induced by a continuously moving interface across the top surface of the cavity, or flows induced by a hydrodynamic imposed shear stress. Most previous studies have assumed that the flow Reynolds number is sufficiently small that a Stokes flow approximation is satisfactory. For example, Alkire and Deligianni (1988) investigated Stokes flow over a cavity for a range of aspect ratios between 0.75 and 10. They found that shallow cavities permit penetration of the outer flow in to the cavity whilst deeper cavities permit only slight penetration. Occhialini and Higdon (1992), who considered the effects of duct inlet flow profile and system geometry, show that a parabolic duct flow allows more penetration into the cavity. They also suggest that the cavity flow is sensitive to system geometry at a critical aspect ratio of about 3. In general, it is suggested that mass transfer is enhanced as the duct flow penetrates more deeply into the cavity.

* Corresponding author.

E-mail address: lcfang@cc.cma.edu.tw (L.C. Fang)

0142-727X/99/$ - see front matter
PII: S0142-727X(99)00050-8

Table 1
A selection of studies of cavity flows

Authors	Flow	Cavity geometry	Re	Method
Kang and Chang (1982)	Poiseuille, steady	Rectangular, AR: 5.0	50–500	Numerical and Experimental
Higdon (1985)	Shear flow, steady	Rectangular and circular, AR: 0.25–4.0	Stokes	Numerical
Shen and Floryan (1985)	Combined Couette and Poiseuille, steady	Rectangular, AR: 0.5–4.0	Stokes	Numerical and experimental
Chang et al. (1987)	Poiseuille, steady	Rectangular, AR: 1.0–10.0	0–300	Numerical and experimental
Alkire et al. (1990)	Poiseuille, steady	Rectangular, AR: 0.75–10.0	Stokes	Numerical and experimental
Yeckel et al. (1990)	Shear flow, steady	Periodic rectangular and triangular	Stokes	Theoretical and experimental
Mickaily et al. (1992)	Couette and Poiseuille, steady	Periodic triangular	Stokes	Numerical and experimental
Occhialini and Higdon (1992)	Couette and Poiseuille, steady	Rectangular	Stokes	Numerical
Pozrikidis (1994)	Shear flow, steady	Rectangular and circular, AR: 0.25–4.0	Stokes	Numerical
Fang et al. (1997)	Poiseuille, steady	Rectangular, AR: 0.25–4.0	50–1600	Numerical and experimental

Some studies, such as those by Kang and Chang (1982) and Chang et al. (1987), have included the effects of the inertia terms which distort the symmetry associated with Stokes flow and which become increasingly important as the Reynolds number increases. These studies, however, are limited to steady flows. Kang and Chang (1982) considered mass transfer from pressure driven cavity flows for Reynolds numbers in the range 20–500. They show how the eddy structure changes with Reynolds number and the effect it has on mass transfer. Chang et al. (1987) considered shear driven flows in deep cavities and show that mass transfer is enhanced mainly by the primary and secondary vortices in the cavity. They also show that the number of vortices increases as the cavity depth increases. Reynolds numbers up to 300 were considered.

There have been many papers on lid-driven cavity flows. Examples of steady solutions using vorticity-streamfunction formulations are those given by Ghia et al. (1982) and by Schreiber and Keller (1983). Others, including Kim and Moin (1985), Soh (1987), Vanka (1986) and Soh and Goodrich (1988), used primitive variables in their formulations of the Navier–Stokes equations. For a square cavity the solutions show a primary central vortex with secondary vortices in each of the two lower corners of the cavity. For deeper cavities the number of main vortices increases.

At the lower corners of a cavity Moffat (1964) has shown that an infinite number of vortices will be present. In practice, however, numerical solutions can only model a finite number of these due to the finite resolution of the flow by the computational mesh. This should not present a problem as it is reasonable to assume that the primary cavity vortices and secondary corner vortices will play the dominant role in the removal of a cavity foulant.

Time-dependent solutions of lid-driven cavity flows using vorticity and velocity as primary unknowns are given by Gatski et al. (1982), and solutions using primitive variables are given by Chen and Chen (1984), Gustafson and Halasi (1986, 1987), Soh and Goodrich (1988) and Goodrich and Soh (1989). In each of these cases the lid on the cavity is started impulsively from rest and attention is focused on the vortex dynamics. Goodrich and Soh (1989), who considered a lid driven square cavity flow with a lid Reynolds number of 1000, showed that a secondary recirculatory vortex develops on the upstream vertical boundary and gradually moves downwards until it coalesces with a second vortex which has developed in the lower corner of the cavity. For a deeper cavity of aspect ratio two, Gustafson and Halasi (1987) show that soon after the start-up the flow in the cavity is symmetrical about the vertical centreline of the cavity with the vortex centre located close to the moving lid. As time progresses a secondary recirculating vortex forms on the upstream boundary and gradually moves downwards to form a second main vortex.

The flow in a two-dimensional cavity driven by an oscillating lid has been considered by Soh and Goodrich (1988) who show that a periodic steady solution is achieved at long times after the initial start-up. Iwatsu et al. (1993) solve the time dependent Navier–Stokes equations for three-dimensional incompressible flow in a cavity with an oscillating lid for Reynolds numbers less than 2000 and lid oscillating frequencies less than 10 rad/s. For sufficiently high frequencies the flow in the bulk of the three-dimensional cavity is similar to the two-dimensional solution, but at low frequencies three-dimensional effects become more pronounced.

Whilst steady state cavity flows and unsteady lid-driven cavity flows have received a considerable amount of attention the unsteady flow of a continuous fluid over a cavity and the corresponding flow in the cavity is less well researched. Some work has been published on unsteady cavity flows where this is related to instability phenomena. For example, Pereira and Sousa (1995) provide a review of work on moderate Reynolds number flows of around 3000 over a shallow cavity. An instability process is described which can lead to self sustained oscillations near the shear layer between the channel and cavity. It is shown that complex coupling between an unstable shear layer and the recirculating cavity flow field can lead to eddy shedding. The topic of cavity cleaning is not considered.

Experimental results presented in this paper show that the cleaning of cavities which contain a foulant with properties not too different from the cleaning fluid is primarily due to flushing by convection during and shortly after the start-up of the duct flow. This particular aspect of the cleaning process has not been considered before and forms the basis of the present study. The diffusive removal of the contaminant becomes increasingly important over a time period which is a few orders of magnitude greater than the start-up time considered in the present study. The contribution from mass diffusion is negligible over the time periods considered and is therefore not included in the analysis.

Understanding of the cleaning process requires an insight into the way in which the secondary flows develop within a cavity. Attention in the present work is focused on the tran-

sient development of a cavity flow which is driven by an accelerating duct flow, the influence of duct flow acceleration on the cleaning rate and the effects of Reynolds number. In the present study the numerical solution of the time dependent, two-dimensional Navier–Stokes equations is achieved by a finite difference formulation using primitive variables and a staggered grid arrangement as first introduced by Harlow and Welch (1965) in their Marker and Cell method. Similar finite difference formulations of the equations of motion for other problems have been used previously by, among others, Miyata and Nishimura (1985), Liu et al. (1990), and Nicolaou et al. (1993, 1995). These studies which cover a variety of fluid flow problems show that the formulation works well for modelling incompressible laminar flows. The finite difference code which has been written for the present investigation has been validated by calculating and comparing lid-driven cavity flows with results of previous studies; the validation results are given by Fang et al. (1997).

In the present study passive markers are introduced into the flow field to enable flow visualisation and measurement of the amount of fluid foulant removed by convection from the cavity; the markers play no part in the flow calculations. The fluid removal process during and shortly after the start-up is compared both qualitatively and quantitatively with experiments.

2. Physical model and numerical method

The geometry of the duct-cavity configuration is shown in Fig. 1. The maximum inlet velocity U and duct height H are used as the characteristic velocity and length scales for the problem so the Reynolds number is defined by $\mathrm{Re} = UH/v$ where v is the kinematic viscosity of the fluid. The Cartesian form of the non-dimensional Navier–Stokes and continuity equations which describe the flow of a two-dimensional, incompressible, viscous and non-diffusive fluid are:

$$\frac{\partial u}{\partial t}+\frac{\partial u^2}{\partial x}+\frac{\partial uw}{\partial z}=-\frac{\partial p}{\partial x}+\frac{1}{\mathrm{Re}}\left(\frac{\partial^2 u}{\partial x^2}+\frac{\partial^2 u}{\partial z^2}\right), \tag{1}$$

$$\frac{\partial w}{\partial t}+\frac{\partial wu}{\partial x}+\frac{\partial w^2}{\partial z}=-\frac{\partial p}{\partial z}+\frac{1}{\mathrm{Re}}\left(\frac{\partial^2 w}{\partial x^2}+\frac{\partial^2 w}{\partial z^2}\right), \tag{2}$$

$$\frac{\partial u}{\partial x}+\frac{\partial w}{\partial z}=0. \tag{3}$$

The flow field is discretized into cells of size $\delta x \times \delta z$ with cell centres being identified by integers i and k in the x and z directions respectively. A staggered placement of variables is used with horizontal velocity components u located on the vertical sides of each cell, vertical components w on the horizontal sides, and pressure p at cell centres. The time derivatives are represented by forward differences and the spatial derivatives by a combination of centred and upstream differencing. For example, if integer n represents the time level, then u at a new $(n+1)$ time level is calculated from

$$\begin{aligned} u^{n+1}_{i+1/2,k} = {} & u_{i+1/2,k} - \delta t\left(UCX_{i+1/2,k} + UCZ_{i+1/2,k}\right) \\ & + \frac{\delta t}{\mathrm{Re}\delta x^2}\left(u_{i+3/2,k} - 2u_{i+1/2,k} + u_{i-1/2,k}\right) \\ & + \frac{\delta t}{\mathrm{Re}\delta z^2}\left(u_{i+1/2,k+1} - 2u_{i+1/2,k} + u_{i+1/2,k-1}\right) \\ & - \frac{\delta t}{\delta x}\left(p_{i+1,k} - p_{i,k}\right)^{n+1}. \end{aligned} \tag{4}$$

Values for terms with no superscript are taken at the nth time level. The convection terms in (4) are given by

$$\begin{aligned} UCX_{i+1/2,k} = \frac{1}{4\delta x}\Big\{ & \left(u_{i+3/2,k.} + u_{i+1/2,k}\right)^2 - \left(u_{i+1/2,k} + u_{i-1/2,k}\right)^2 \\ & - \alpha\left|u_{i+3/2,k} + u_{i+1/2,k}\right|\left(u_{i+3/2,k} - u_{i+1/2,k}\right) \\ & + \alpha\left|u_{i+1/2,k} + u_{i-1/2,k}\right|\left(u_{i+1/2,k} - u_{i-1/2,k}\right)\Big\} \end{aligned} \tag{5}$$

and

$$\begin{aligned} UCZ_{i+1/2,k} = \frac{1}{4\delta z}\Big\{ & \left(w_{i,k+1/2} + w_{i+1,k+1/2}\right)\left(u_{i+1/2,k} + u_{i+1/2,k+1}\right) \\ & - \alpha\left|w_{i,k+1/2} + w_{i+1,k+1/2}\right|\left(u_{i+1/2,k+1} - u_{i+1/2,k}\right) \\ & - \left(w_{i+1,k-1/2} + w_{i,k-1/2}\right)\left(u_{i+1/2,k-1} + u_{i+1/2,k}\right) \\ & + \alpha\left|w_{i,k-1/2} + w_{i+1,k-1/2}\right|\left(u_{i+1/2,k} - u_{i+1/2,k-1}\right)\Big\}, \end{aligned} \tag{6}$$

where α is a combination factor; $\alpha = 0$ gives centred differencing and $\alpha = 1$ gives upstream differencing. A value of 0.5 is used which is sufficient to avoid instabilities arising from numerically introduced negative diffusion (Miyata and Nishimura, 1985). Where a variable is not explicitly defined on the grid then a simple average is calculated from adjacent values. For example, $u_{i+1,k} = \left(u_{i+3/2,k} + u_{i+1/2,k}\right)/2$.

A time-dependent solution is obtained by advancing the flow field through a sequence of short time steps. The iterative method used to converge the calculation at each time level is based upon the method of Chorin (1968) which involves a simultaneous iteration on pressure and velocity. If $D^{n+1}_{i,k}$ represents the divergence of the fluid in a cell where

$$\left(D^{n+1}_{i,k}\right) = \frac{1}{\delta x}\left(u^{n+1}_{i+1/2,k} - u^{n+1}_{i-1/2,k}\right) + \frac{1}{\delta z}\left(w^{n+1}_{i,k+1/2} - w^{n+1}_{i,k-1/2}\right), \tag{7}$$

then the pressure $p^{n+1}_{i,k}$ in that cell is adjusted in a way that drives the divergence in all cells towards zero. The pressure is updated using

$$\left(p^{n+1}_{i,k}\right)^{m+1} = \left(p^{n+1}_{i,k}\right)^{m} - \beta\left(D^{n+1}_{i,k}\right)^{m}, \tag{8}$$

where m indicates the mth sweep of the mesh and 'β' is a relaxation parameter. The solution is reached when the magnitude of $D^{n+1}_{i,k}$ in each cell is less than some pre-set small value, typically O(10^{-6}). No-slip boundary conditions are applied at all solid boundaries, a flow velocity is prescribed at the inflow boundary and zero normal gradients are used to set variables just outside the outflow boundary.

Flow visualisation and fluid contamination calculations are made possible by the use of passive markers. These are initially distributed before start-up and are moved to new positions at each time step. For example the new x-position of a marker k at time level $(n+1)$ is calculated from $x^{n+1}_k = x^n_k + u^{n+1}_k \delta t$, where u_k is the horizontal velocity at the marker position, x^n_k. The velocity components at the marker positions are calculated by

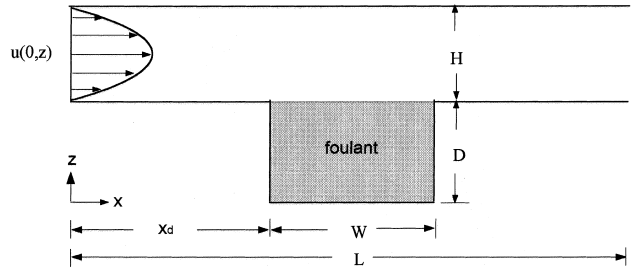

Fig. 1. The coordinate system for a duct-cavity set-up.

a weighted interpolation of velocities in surrounding cells as described by Welch et al. (1966).

Approximate stability conditions for the method used have been provided by Miyata and Nishimura (1985) and place restrictions on the time step and the combination factor, α:

$$\left(\frac{\delta t}{\delta x}u+\frac{\delta t}{\delta z}w\right)\leqslant\alpha\leqslant 1 \quad \text{and} \quad v\leqslant\frac{1-\alpha((\delta t/\delta x)u+(\delta t/\delta z)w)}{2\delta t(1/\delta x^2+1/\delta z^2)}.$$

Only the first of these two conditions imposes a restriction for the present problem; the second condition becomes restrictive only for highly viscous flows. The time steps chosen for the present flow problems generally satisfied $\delta t\leqslant\alpha\delta x/U$ which proved to be a sufficient condition for numerical stability.

The computer code has been validated by application to two different types of problem for which solutions are available. The first test was with a steady lid-driven cavity flow when $\mathrm{Re}=400$ as considered by Ghia et al. (1982). Comparing flow velocities from the present method with those from Ghia et al. gave good agreement with differences being of the order of 1% or less. The second test was a numerical simulation of a time dependent collapse of a uniformally mixed region in a linearly stratified fluid as considered experimentally by Wu (1969). For this problem the density equation was included in the formulation to account for the density stratification. Measuring the length of the mixed region at different times and comparing with the experimental results of Wu (1969) the differences were typically less than 2% at early times, but increased after a long time when the thickness of the collapsed region had decreased to an order of magnitude equal to a cell height. This was consistent with the observations of Young and Hirt (1972) in their numerical study of the same problem. Doubling the number of cells and halving the time step had little effect on the results at the early times but did improve the results when the width of the mixed region became small.

For the problem of a duct flow over a cavity the maximum cell size used was 0.02×0.02 and the time step never exceeded $\delta t=0.01$ for the range of Reynolds numbers considered. Values less than these had negligible effect on the overall results obtained, but smaller cell sizes did improve the resolution of the smaller vortices in the cavities.

3. Flow characteristics

To understand the way in which a cavity can be purged, it is first necessary to see how the flow develops as the duct fluid accelerates from rest to some prescribed duct flow Reynolds number. In most of the ensuing discussion the entry profile to the duct is always assumed to be parabolic and the start-up flow velocity varies as

$$u=1-(1+at)^{-1},$$

where the parameter a determines the magnitude of the acceleration. Except where stated otherwise, the value used is $a=10$.

For ratios of cavity depth to duct height, D/H, between 1 and 4, numerical tests have shown almost no change in the cavity flow characteristics after steady flow conditions are reached. However, the value of D/H can influence the percentage of contaminated fluid trapped in a cavity for aspect ratios greater than one. Further details are given in Section 4.

The development of vortices in a deep cavity as time progresses is shown in Fig. 2. For $\mathrm{AR}=0.25$ and $\mathrm{Re}=50$. At the beginning of the flow development the streamline contours tend to be symmetrically spaced about the centreline of the cavity since the Reynolds number based on the instantaneous maximum inflow velocity is within the Stokes flow range. At later times vortices form, and it has been observed that decreasing the aspect ratio leads to more vortices forming, with the bottom vortex becoming weaker as the cavity depth increases. It may be anticipated that under such conditions the scouring of the bottom of a cavity becomes negligible for very deep cavities. In their steady flow study Chang et al. (1987) suggest that in such deep cavities only the top two vortices affect mass transfer.

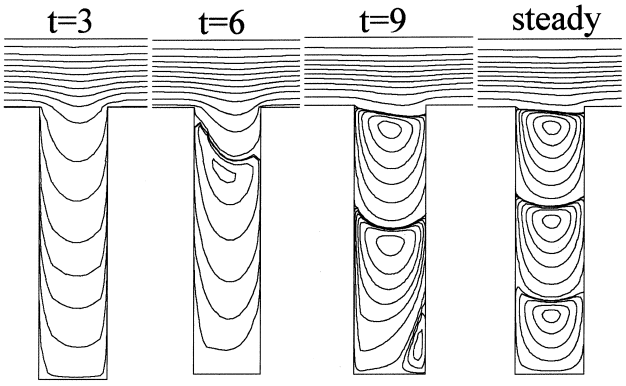

Fig. 2. Cavity flow development for $\mathrm{AR}=0.25$ and $\mathrm{Re}=50$.

Streamlines for two cavities of aspect ratios $\mathrm{AR}=1$ and 4, and with $\mathrm{Re}=50$, are shown in Fig. 3. For $\mathrm{AR}=1$, a primary vortex begins to form at about $t=4$ and develops into a single large vortex by the time the flow is essentially steady. The centre of the vortex is located about three quarters of the cavity depth from the bottom and at mid-width. The flow velocities associated with the vortex are greater in the upper portion of the cavity. This is broadly in agreement with the results of Burggraf (1966). In practice a pair of small and weaker counter-rotating vortices develop in the lower corners of the cavity which are not resolved by the size of the grid spacing used in the present calculations. For $\mathrm{AR}=4$, a main vortex forms at the upstream wall of the cavity, very much like a flow over a backward facing step.

The transient streamline patterns shown in Figs. 2 and 3 suggest that at the early stages after start-up, the external flow has a tendency to penetrate to the bottom of the cavity. For $\mathrm{AR}=4$ the flow penetration to the bottom of the cavity remains beyond the start-up stage, eventually leaving one large main vortex in the upstream corner of the cavity; smaller un-

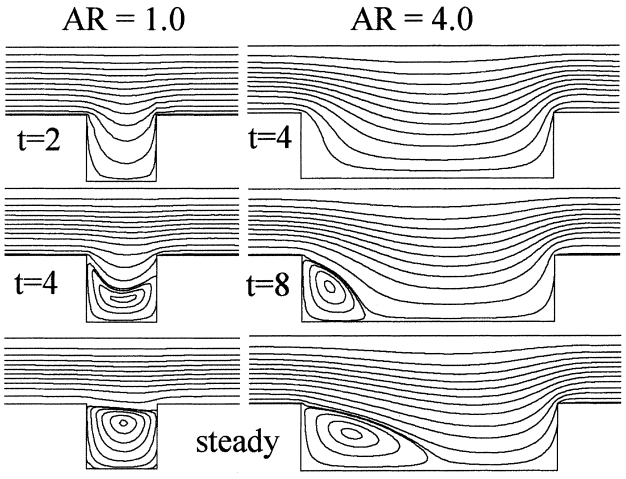

Fig. 3. Cavity flow development for $\mathrm{AR}=1$ and 4, $\mathrm{Re}=50$.

resolved vortices exist close to the lower corners of the cavity. This penetration of the external flow has been noted for steady Stokes flow by Shen and Floryan (1985) and Higdon (1985). A similar penetration has been noted for steady flows at higher Reynolds numbers by Kang and Chang (1982), and they also show that the movement of the stagnation point on the bottom of the cavity gives rise to increased mass transfer at the bottom wall of the cavity. The final flow pattern, and therefore the cleaning effectiveness, will depend on the flow Reynolds number which determines the degree of penetration of the duct flow into the cavity. But it is reasonable to expect that the cleaning process will also be affected by the acceleration of the flow to its steady state.

Fig. 4 illustrates the flow development over a cavity with AR = 4 following an instantaneous start of the duct flow to a Reynolds number of Re = 400. Numerical calculations have shown that the flow patterns initially (up to about $t = 1$) resemble stokes flow and by $t = 6$ a main vortex forms at the upstream wall of the cavity. Deep penetration of the outer flow only occurs at the earliest times and it is this motion which is mainly responsible for purging of the contaminated cavity fluid. Following the initial Stokesian flow and the early stages in the development of the main vortex, considerable mixing of the cavity fluid then occurs via one single vortex occupying the entire cavity when steady state conditions have been reached. For the conditions applying to Fig. 4, the steady state flow was fully established by a nondimensional time of 40.

To assess the effect of flow acceleration on the intermediate flow patterns, a linear flow acceleration from rest is considered such that

$$\mathrm{Re} = 400\ (t/t_\mathrm{m}) \quad \text{for} \quad 0 < t < t_\mathrm{m},$$
$$\mathrm{Re} = 400 \quad \text{for} \quad t \geqslant t_\mathrm{m},$$

where t is nondimensional time and t_m represents the nondimensional time it takes for the flow Reynolds number to reach 400. The streamlines for instantaneous Re values of 50, 100 and a final value of 400 are shown in Fig. 5 for $t_\mathrm{m} = 0.4$ and 40. The flows at the instantaneous Re values for the fast acceleration are not the same as the steady state flow patterns at the corresponding Reynolds numbers. For instance, the flow streamline patterns for Re = 400 shown in the column corresponding to $t_\mathrm{m} = 0.4$ resemble those for a steady state flow at Re = 50. These observations are due to the time required for the fluid to overcome its inertia and to adjust to the new flow parameter values. The acceleration corresponding to $t_\mathrm{m} = 40$ is sufficiently slow to enable the flow to adjust and, therefore, the flow patterns at the instantaneous Re values for $t_\mathrm{m} = 40$ resemble closely the steady flow patterns at the corresponding steady Reynolds numbers.

Steady flows over cavities with AR = 4, and for Re = 50, 100 and 400, resemble closely those that appear in Fig. 5 when $t_\mathrm{m} = 40$. Clearly, the flow patterns are influenced by Reynolds

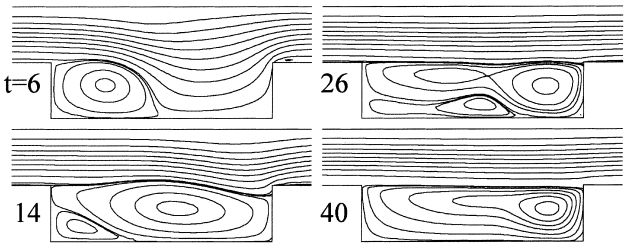

Fig. 4. The transient development of a cavity flow for Re = 400 and AR = 4, after an instantaneous start of the duct flow. Numbers represent nondimensional time.

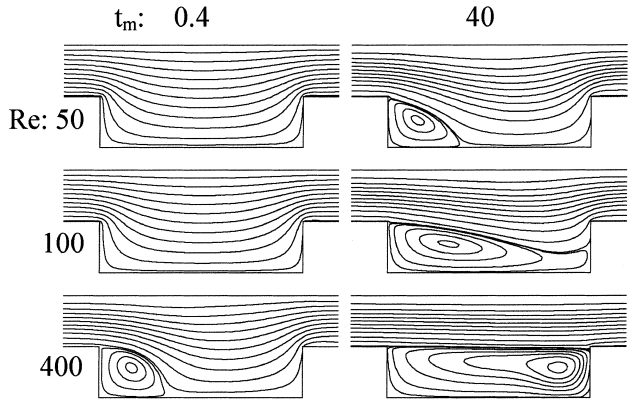

Fig. 5. Linear acceleration to a maximum Re = 400, t_m represents the time to reach maximum Re. Each row corresponds to the indicated instantaneous duct Re attained during the acceleration. Each column represents a different duct flow acceleration.

number. The closed circulation region has a much reduced area at the lower Reynolds number of 50, and it is reasonable to expect that the amount of contaminated fluid remaining in the cavity will be related to this area of recirculating fluid. The analysis that follows shows that, in addition to the dependence on the final Reynolds number and the steady state flow pattern, the time dependent development of the flow to the steady state also has a significant effect on the amount of contaminated fluid that is removed from a cavity.

4. Contaminated fluid removal from a cavity

When recirculating regions are formed in a cavity during the flow start-up they entrap part of the contaminated fluid that initially resided in the cavity; the remainder contaminated fluid will be flushed by the cavity penetrating duct flow. By measuring the area covered by the recirculating fluid in the cavity it is possible to estimate the fraction of a cavity area that will contain contaminated fluid soon after a steady state is reached. The concentration of contaminant in this recirculating region will differ from that existing in the cavity initially, and will depend on how the flow established itself in the cavity. Further discussion on this topic is included later in this paper. For now, attention is focused on the fraction of cavity area occupied by contaminated fluid when the flow has reached its steady state, regardless of contaminant concentration.

Fig. 6(a) shows the fraction of the cavity area containing contaminated fluid when the flow reaches its steady state. The area enclosed by the recirculating fluid in a cavity is represented by A_ψ and its value is the area enclosed by the cavity walls and the streamline separating the recirculating region from the duct flow. In general, the value of A_ψ is close to the value of the total cavity area, A_c, when the cavity aspect ratio is small and the duct flow Reynolds number is large. With these conditions any contaminant left in the cavity following the start-up of the flow will only be further removed by convection enhanced diffusion as demonstrated by Chilukuri and Middleman (1983).

The effect of the ratio of cavity depth to duct height, D/H, on the percentage of fluid trapped in the cavity is shown in Fig. 6(b). For a given aspect ratio of one or less the ratio D/H has little effect on the removal of contaminated fluid, and the percentage of contaminated fluid remaining in the cavity is relatively high. For larger aspect ratios the amount of contaminated fluid trapped in the cavity decreases as D/H decreases.

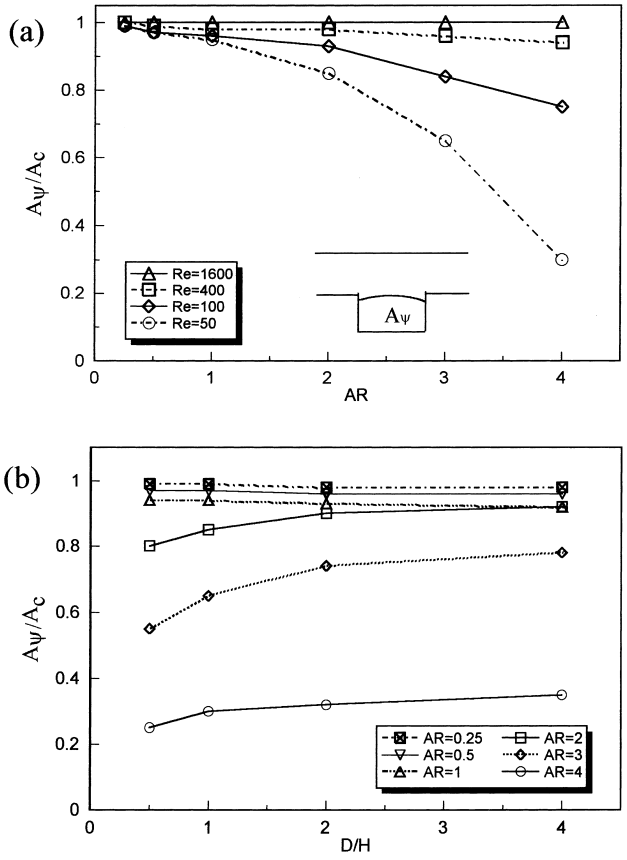

Fig. 6. Fraction of cavity area containing contaminated fluid plotted against: (a) cavity aspect ratio; (b) against D/H.

Steady state solutions of the flow over a cavity, as developed by Yeckel et al. (1990) and Mickaily et al. (1992), as well as those presented in this paper, can predict the fraction of a cavity that may contain contaminated fluid; but streamline patterns do not indicate how much of the contaminant is removed nor the process by which it is removed. To evaluate this a number of passive markers are introduced in the cavity prior to initiating the flow. The motion of each marker was recorded as the duct flow interacted with that in the cavity. Trial and error showed that 1600 markers uniformly distributed through the cavity enabled a good picture of the flow to be realised. The use of marker particles achieves the same effect as adding a diffusion equation in which the diffusivity is taken as zero, and therefore the movement of the markers is entirely due to convection. The use of passive markers has the advantage of graphically showing how fluid is exchanged between the duct and the cavity.

Fig. 7 shows markers which represent contaminated fluid, and it shows how the contaminated fluid is displaced from the cavity when the Reynolds number is 50. The corner vortices which form, as shown in the streamline patterns of Fig. 3, confine some of the markers in the cavity. Fig. 8, which illustrates the initial position of the markers which are eventually removed from a cavity, suggests that most of the contaminated fluid is removed from the upper downstream end of the cavity. The path traces of two individual markers as they are carried by the fluid are shown in Fig. 9 for $Re = 50$, 400 and 1600. The paths illustrate the tortuous nature by which a contaminated fluid element may be either ejected from the cavity or become permanently trapped in the cavity.

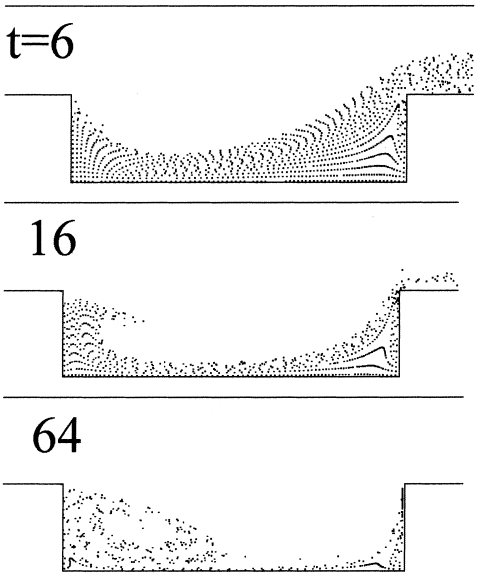

Fig. 7. The removal process of contaminated cavity fluid when $AR = 4$ and $Re = 50$. The contaminated fluid is represented by passive markers particles.

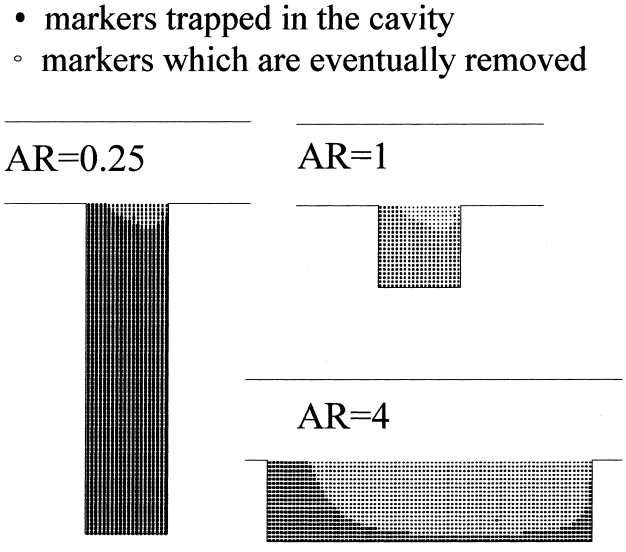

Fig. 8. The initial positions of markers which remain or are removed from the cavity after a steady state flow has been reached.

The percentage of markers removed as time progresses for $AR = 4$ and $Re = 50$ is given in Fig. 10(a). Of particular interest is the way in which the removal depends on the start-up time of the duct flow. In the early phases of the motion it is clear that the percentage of markers removed increases as the acceleration of the fluid increases, but for longer times the influence of the start-up time is fairly small. This is a significant result from the cleaning point of view since it will affect the maximum amount of contaminant that can be removed and provide the basis of assessing the very long term removal when convection enhanced diffusion takes over.

An insight into the physics by which a higher percentage of markers is removed when the fluid acceleration is high is provided by the instantaneous streamline patterns shown in Fig. 5. At the same instant, shortly after flow start-up, a higher

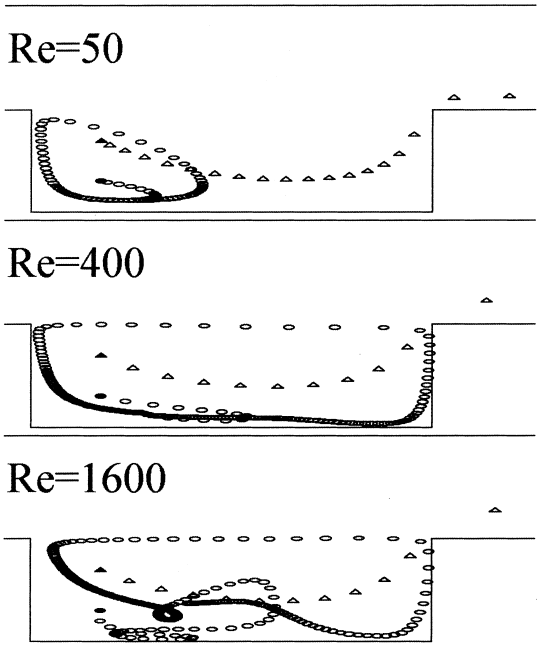

Fig. 9. Path-traces of two markers in a cavity with AR = 4 for different Reynolds numbers.

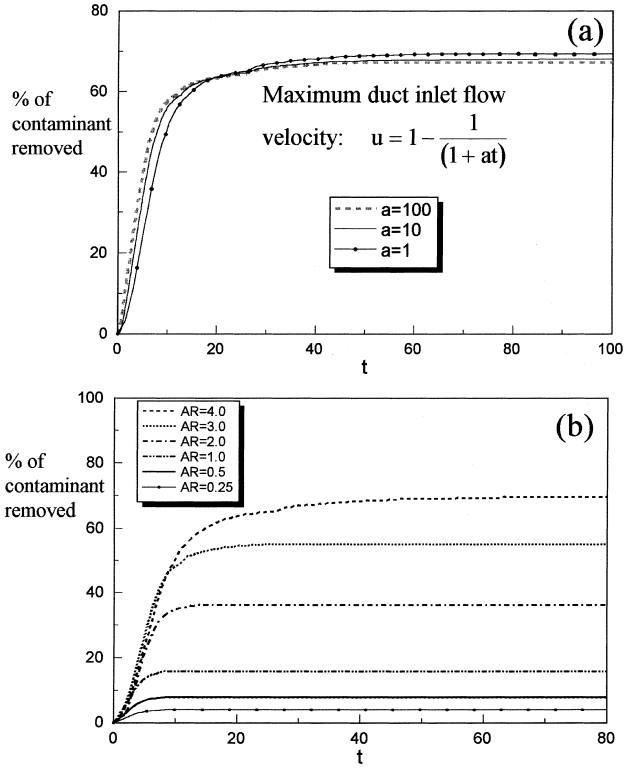

Fig. 10. Percentage of contaminant (markers) removed from a cavity with time for Re = 50, (a) influence of start-up acceleration for a cavity with AR = 4, (b) influence of cavity AR ($a = 10$).

acceleration will produce higher velocities in the cavity. These higher velocities, coupled with the penetration of the duct flow to the bottom of the cavity, results in the removal of a greater number of markers from the cavity than would be the case if the flow velocities in the cavity were lower.

Fig. 10(b) shows the percentage of markers (based on the total number of markers in the cavity before flow start-up) removed from cavities of different AR against time. No further removal of contaminant occurs after the steady state vortex system becomes established. Over the range of aspect ratios considered the percentage removed varies almost linearly with AR. Within the scope of the present calculations a maximum of about 70% can be removed when AR = 4, but this value will increase as AR increases; the limit would represent the removal of foulant from a backward facing step.

Numerical experiments have shown that, for the same AR and flow acceleration, the final percentage of markers removed also increases as the Reynolds number increases. This is also due to the higher velocities in the cavity and the form of the streamlines as explained earlier.

5. Experimental flow visualisation

To validate the computer model a limited number of flow visualisation pictures were undertaken. A rectangular water duct with dimensions of 35 mm × 15 mm was fitted with cavities of varying aspect ratio, and a depth equal to the duct height. The fluid in the cavity was dyed and assumed to behave in a way similar to that of the theoretical markers. This is a good assumption provided the time period of the event is sufficiently short for molecular diffusion and to be

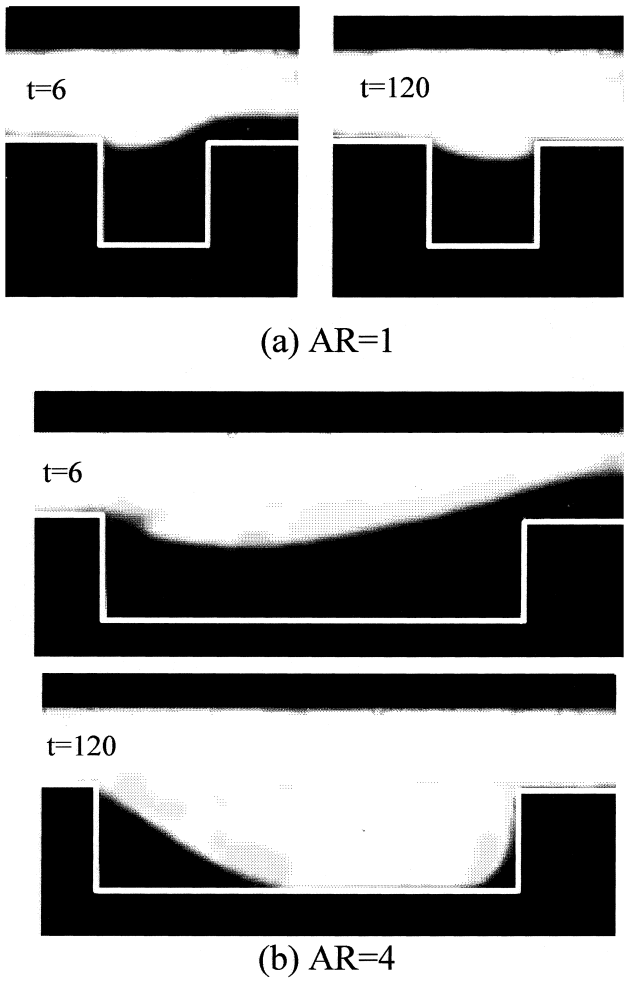

Fig. 11. Experimental results of cavity fluid displacement for Re = 50.

insignificant. Time elapsed photographs were taken following flow start-up. The time taken to physically open the flow valve for the images shown in Fig. 11. was about 5 s (nondimensional time = 1) which is much less than the nondimensional times of 6 and 120 at which the photographs were taken. The start-up time in the experiments was of the same order of magnitude as the numerical calculations. Comparing the experimental dye solution position for the AR = 4 case with the marker movement simulation in Fig. 7 shows good qualitative agreement. The results clearly demonstrate how the purging of the contaminated cavity fluid increases as the aspect ratio increases.

In the early phases of the flow, and for the lower Reynolds numbers, the percentage of contaminated fluid elements remaining in the cavity corresponds roughly to the percentage of the cavity area containing dyed solution. This is due to diffusion having negligible effect at these early times, and the fluid originally in the cavity becoming trapped in the recirculating regions with little change in the concentration of the dye. This is reflected in the good agreement between theory (based on the number of markers) and experiment as shown in Fig. 12(a) for Re = 50. A long time after the start the effects of diffusion (which has not been included in the numerical analysis) and the fact that the trapped contaminant in the cavity will occupy a greater volume, means that the analysis based on the number of markers has little bearing on the area occupied the dyed fluid.

Fig. 12(b) compares the experimental estimate of the fluid trapped in the cavity (based on the area covered by the dye solution interface) with the calculations for different Re. Agreement between experiment and numerical simulation based on marker numbers is reasonable only for small Reynolds number. This is a result of the concentration of the contaminant in the trapped fluid becoming less with time. When the percentage of cavity area covered by the markers in the numerical simulation is compared with the percentage of cavity area covered by the dye solution in the experiments then the agreement is much improved. Information on the concentration of the contaminant, however, is limited.

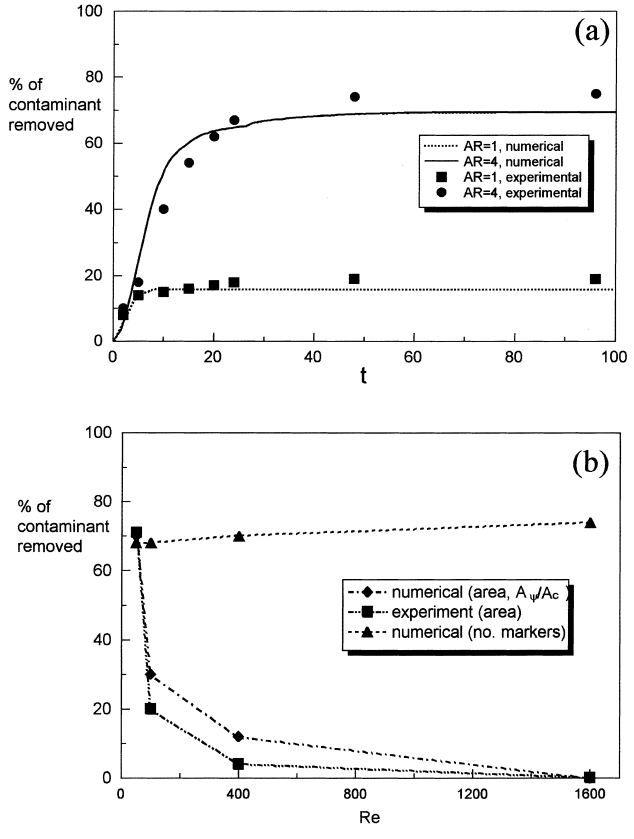

Fig. 12. The percentage of contaminated fluid removed from a cavity: comparison between numerical solutions and experiment: (a) Re = 50, the 'numerical' values are based on the number of markers in the cavity, (b) the effect of Reynolds number.

6. Conclusions

Laminar flow solutions for parabolic flow over a rectangular cavity have illustrated the effect of inertia on the transient development of the flow over a cavity and have shown how fresh duct fluid purges contaminated fluid from the cavity. The rate at which the contaminated cavity fluid is removed is relatively high during the unsteady start-up of the duct flow and approaches zero after the flow reaches a steady state. The cleaning process is enhanced as the cavity aspect ratio is increased and as the duct Reynolds number increases. A prolonged cleaning process after steady flow conditions have been reached is shown to be ineffective in further purging of contaminated fluid from a cavity since removal by convection is negligible and any further cleaning will be almost entirely due to convection enhanced diffusion.

A 'volumetric' approach based on the spread of markers is shown to be useful in determining the fraction of the cavity that remains contaminated after steady conditions have been reached. Markers are used to show the regions in a cavity which are occupied by trapped contaminated fluid after steady flow conditions are reached. As AR increases, the dominant regions are located increasingly near the upstream side of a cavity where the closed streamlines are formed. Flow visualisation experiments justify the main findings of the numerical simulations.

References

Alkire, J.K., Deligianni, H., 1988. The role of mass transfer on anisotropic electrochemical pattern etching. J. Electrochemical Soc. 135, 1093–1100.

Alkire, J.K., Deligianni, H., Ju, J.B., 1990. Effect of fluid flow on convective transport in small cavities. J. Electrochemical Soc. 137, 818–824.

Burggraf, O., 1966. Analytical and numerical studies of the structure of steady separated flows. J. Fluid Mech. 24, 113–151.

Chang, H.N., Ryu, H.W., Park, D.H., Park, Y.S., 1987. Effect of external laminar channel flow on mass transfer in a cavity. Int. J. Heat Mass Transfer 30, 2137–2149.

Chen, C.J., Chen, H.C., 1984. Finite analytical numerical-method for unsteady 2-dimensional Navier–Stokes equations. J. Comput. Phys. 53, 209–226.

Chilukuri, R., Middleman, S., 1983. Circulation, diffusion and reaction within a liquid trapped in a cavity. Chem. Eng. Commun. 22, 127–138.

Chorin, A.J., 1968. Numerical solution of the Navier–Stokes equations. Math. Comput. 22, 745–762.

Fang., L.C., Cleaver, J.W., Nicolaou, D., 1997. Hydrodynamic cleaning of cavities. In: Proceedings Comp. Methods and Exp. Methods VIII, pp. 391–401.

Gatski, T.B., Grosch, C.E., Rose, M.E., 1982. A numerical study of the two-dimensional Navier–Stokes equations in vorticity-velocity variables. J. Comput. Phys. 48, 1–22.

Ghia, U., Ghia, K.N., Shin, C.T., 1982. High-re solutions for incompressible flow using the Navier–Stokes equations and a multigrid method. J. Comput. Phys. 48, 387–411.

Goodrich, J.W., Soh, W.Y., algorithms, J., 1989. Time-dependent viscous incompressible Navier–Stokes equations: the finite difference Galerkin formulation and stream function. Comput. Phys. 84, 207–241.

Gustafson, K., Halasi, K., 1986. Vortex dynamics of cavity flow. J. Comput. Phys. 64, 279–319.

Gustafson, K., Halasi, K., 1987. Cavity flow dynamics at higher Reynolds-number and higher aspect ratio. J. Comput. Phys. 70, 271–283.

Harlow, F.H., Welch, J.E., 1965. Numerical calculation of time-dependent viscous incompressible fluid with a free surface. Phys. Fluid 8, 2182–2189.

Higdon, J.L., 1985. Stokes flow in arbitrary two-dimensional domains. J. Fluid Mech. 159, 195–226.

Iwatsu, R., Hyun, J.M., Kuwahara, K., 1993. Numerical simulations of three-dimensional flows in a cubic cavity with an oscillating lid. J. Fluids Eng. Trans. ASME 115, 680–686.

Kang, I.S., Chang, H.N., 1982. The effect of turbulence promoters on mass transfer-numerical analysis and flow visualisation. Int. J. Heat Mass Transfer 25, 1167–1181.

Kim, J., Moin, P., 1985. Application of a fractional-step method to incompressible Navier–Stokes equations. J. Comput. Phys. 59, 308–323.

Liu, R., Nicolaou, D., Stevenson, T.N., 1990. Waves from an oscillatory disturbance in a stratified shear flow. J. Fluid Mech. 219, 609–619.

Mickaily, E.S., Middleman, S., 1993. Hydrodynamic cleaning of a viscous fluid from the inside of a long tube. AIChE J. 39, 885–893.

Mickaily, E.S., Middleman, S., Allen, M., 1992. Viscous flow over periodic surfaces. Chem. Eng. Commun. 117, 401–414.

Miyata, H., Nishimura, S., 1985. Finite-difference simulation of non-linear ship waves. J. Fluid Mech. 157, 327–357.

Moffat, M.K., 1964. Viscous and resistive eddies near a sharp corner. J. Fluid Mech. 18, 1–18.

Nicolaou, D., Garman, J.F.R., Stevenson, T.N., 1995. Internal waves from a body accelerating in a thermocline. Appl. Sci. Res. 55, 171–186.

Nicolaou, D., Liu, R., Stevenson, T.N., 1993. The evolution of sheared and nonsheared thermocline waves from an oscillatory disturbance. J. Fluid Mech. 254, 401–416.

Occhialini, J.M., Higdon, J.J.L., 1992. Convective mass transport from rectangular cavities in viscous flow. J. Electrochemical Soc. 139, 2845–2855.

Pereira, J.C.F., Sousa, J.M.M., 1995. Experimental and numerical investigation of flow oscillations in a rectangular cavity. J. Fluids Eng. Trans. ASME 117, 68–74.

Pozrikidis, C., 1994. Shear flow over a plane wall with an axisymmetrical cavity or a circular orifice of finite thickness. Phys. Fluids 6, 68–79.

Schreiber, R., Keller, H.B., 1983. Spurious solutions in driven cavity calculations. J. Comput. Phys. 49, 165–172.

Shen, C., Floryan, J.M., 1985. Low Reynolds number flows over cavities. Phys. Fluids 28, 3191–3202.

Soh, W.Y., 1987. Time-marching solution of incompressible Navier–Stokes equations for internal flow. J. Comput. Phys. 70, 232–252.

Soh, W.Y., Goodrich, J.W., 1988. Unsteady solution of incompressible Navier–Stokes equations. J. Comput. Phys. 79, 113–134.

Vanka, S.P., 1986. Block-implicit multigrid solution of Navier–Stokes equations in primitive variables. J. Comput. Phys. 65, 138–158.

Welch, J.E., Harlow, F.H., Shannon, J.P., Daly, B.J., 1966. The MAC method – A computing technique for solving viscous, incompressible, transient fluid-flow problems involving a free surface. Los Alamos Scientific Lab. Rep. LA-3425, Los Alamos.

Wu, J., 1969. Mixed region collapse with internal wave generation in a density stratified medium. J. Fluid Mech. 35, 531–544.

Yeckel, A., Middleman, S., Klumb, L.A., 1990. The removal of thin film from periodical grooved surfaces by an impinging jet. Chem. Eng. Commun. 96, 69–79.

Young, J.A., Hirt, C.W., 1972. Numerical calculation of internal wave motion. J. Fluid Mech. 56, 265–276.